national accelerator laboratory

TM-333
0300

EFFECTS OF NONLINEARITIES ON THE PHASE MOTION IN THE NAL BOOSTER

W. W. Lee

December 1, 1971

There is no good approximate analytic solution for the nonlinear longitudinal phase motion in a synchrotron in regions where the motion is nonadiabatic. In this report, the phase motion in the NAL booster is studied numerically by following an ensemble of particles in the computer. The main interest is in the "adiabatic" rf capture and the transition crossing processes in the presence of nonlinear rf forces. The second-order effect of the momentum spread on the phase motion in the neighborhood of transition is also included in the analysis.

The phase motion of each individual particle is given by the following equations

$$\frac{d\psi}{dt} = h(\omega_s - \omega) \tag{1}$$

$$\frac{dw}{dt} = \frac{ev}{2\pi h}\left[-\sin(\phi_s+\psi) + \sin\phi_s\right] \tag{2}$$

Operated by Universities Research Association Inc. Under Contract with the United States Atomic Energy Commission

where

h = rf harmonic number

ϕ_s = synchronous rf phase

ψ = deviation of particle rf phase from ϕ_s

ω = particle frequency = $c\beta/R$

ω_s = synchronous particle frequency

R = particle orbit radius

w = "conjugate" momentum variable to $\psi = W-W_s = -\frac{R_s}{h}(p-p_s)$

p = particle momentum.

Expanding the particle frequency ω about its synchronous value, we obtain

$$\omega(W) = \omega_s + \left(\frac{d\omega}{dW}\right)_s w + \frac{1}{2}\left(\frac{d^2\omega}{dW^2}\right)_s w^2. \tag{3}$$

Higher order terms are of no interest here, and, therefore, neglected. The coefficients in the above expansion are related to the lattice structure of the machine. Assuming that the synchronous particle moves along a path with an orbit radius R_s and considering a particle with a momentum of $p_s + \Delta p$, we can write down the difference in their orbit radii as

$$\frac{\Delta R}{R_s} = \alpha_1 \frac{\Delta p}{p_s}\left(1 + \alpha_2 \frac{\Delta p}{p_s}\right). \tag{4}$$

Again, the higher order terms are neglected. The coefficient α_1 is the so called "momentum compaction factor," and the coefficient α_2 is generally determined by the second order kinematic as well as magnetic properties of the lattice.

Using the definition of Eq. (4), it can easily be shown that

$$\left(\frac{d\omega}{dW}\right)_s = -\frac{h}{mR_s^2\gamma_s}\,\Lambda \tag{5}$$

and

$$\left(\frac{d^2\omega}{dW^2}\right)_s = -\frac{2h^2\beta_s}{m^2cR_s^3}\left[\frac{3/2}{\gamma_s^4} + \frac{\alpha_2 + 3\Lambda/2}{\left(\gamma_s^2-1\right)\gamma_t^2}\right] \tag{6}$$

where

γ_t = transition energy in mc^2 units = $\alpha_1^{-1/2}$

γ_s = synchronous energy in mc^2 units

$\Lambda = \frac{1}{\gamma_s^2} - \frac{1}{\gamma_t^2}$.

Substituting the above results into Eqs. (1) and (2), and rewriting them on a turn-by-turn integration basis, we obtain

$$\psi_{n+1} = \psi_n + 2\pi h\left[\frac{\Lambda_n}{\left(\gamma_{s,n}^2-1\right)^{1/2}}\,\bar{w}_n + \left[\frac{3/2}{\gamma_{s,n}^4} + \frac{\alpha_2+3\Lambda n/2}{\left(\gamma_{s,n}^2-1\right)\gamma_t^2}\right]\bar{w}_n^2\right] \tag{7}$$

$$\bar{w}_{n+1} = \bar{w}_n + \frac{ev_{n+1}}{mc^2}\,\frac{\gamma_{s,n+1}}{\left(\gamma_{s,n+1}^2-1\right)^{1/2}}\left[\sin\phi_{s,n+1} - \sin\left(\phi_{s,n+1} + \psi_{n+1}\right)\right] \tag{8}$$

where $\bar{w} = w\Big/\left(\frac{mcR_s}{h}\right)$ and subscript n is the revolution number. These equations, which accurately represent a physical situation of a single accelerating gap in the ring, are the basis for our computer experiment. The space-charge forces are not included here. For the NAL booster, we have the following parameters, h = 84,

R_s = 75.47m, γ_t = 5.446, α_2 = 0.843. The coefficient α_2 is calculated by using TRANSPORT (Brown) code. The magnet parameters for the booster are taken from Ref. 1. Neglecting the sextupole contribution of the booster gradient magnets, the second-order kinematic effect alone gives α_2 = 1.63. It is interesting to observe that the coefficient of $\bar{w}$ term in Eq. (7) vanishes at transition, whereas the coefficient of $\bar{w}^2$ term remains nonzero.

At injection, we assume the 200-MeV linac beam to have a momentum spread of $\Delta p/p = \pm 0.8 \times 10^{-3}$ and neglect the 200 MHz bunching. We first populated the (ψ,w) phase space accordingly with 1000 particles, and then performed a 120-turn ($\cong$ 355 μsec) "adiabatic" rf trapping with a final cavity voltage of 100 kV. We observed that all the particles were captured at the end of the trapping with no appreciable increase in the beam phase-space area. The final rf bucket is about 70% filled. The initial and final (ψ, w) phase plots are shown in Fig. 1. We have also studied cases with faster turns-ons. The results show some increases in the beam phase-space area. A more comprehensive study of the rf capture in the booster has been reported by MacLachlan.[2]

The accelerating cycle in the booster lasts 33.333 msec (1/30 sec) with a final beam energy of 8 BeV. Under conditions of constant bucket area and sinusoidal energy gain per turn, Snowdon[3] has calculated the voltage programs for various bucket filling factors (= beam area/bucket area). These programs are shown in Fig. 2 for bucket filling factors of 0.5 and 0.7. Since

his calculation has been carried out under the adiabatic assumption, the voltage program for the region near transition should be modified. Once the particular program is determined, one can then calculate the coordinates for each particle using Eqs. (7) and (8) for the whole accelerating cycle. The results for several different cases we have investigated are outlined below.

A. The voltage program for the bucket filling factor of 0.7 was utilized for the computation except for the region near transition, where we followed curve A of Fig. 2. The time variation of the corresponding synchronous rf phase for the acceleration together with the usual phase jump at transition is also shown in Fig. 2. Since the beam phase-space area is pretty well matched to the rf bucket at the beginning of the acceleration, it remains matched throughout the adiabatic region before transition. In the neighborhood of transition where the motion is nonadiabatic, the beam is sharply bunched and becomes grossly mismatched (if rf bucket still has any meaning at all in this region, see Appendix). Because of the nonlinear rf forces and the second-order effect of the momentum spread in the region of transition crossing, the mismatch persists into the adiabatic region after transition. Filamentation in the phase space follows. This results in a 20% increase in the beam area together with about 10% beam loss at the end of the acceleration.

The final momentum spread is about $\pm 0.29 \times 10^{-3}$. The beam loss can be attributed to the insufficient rf bucket area after transition. The phase distribution plots are shown in Fig. 3.

B. In order to minimize the beam loss, we replaced the voltage program after transition by that corresponding to the bucket filling factor of 0.5 along with curve B, as shown in Fig. 2. The beam loss is considerably reduced to about 2.4%, however, the increase in phase-space area due to filamentation rises to 35%. The final momentum spread is about $\pm 0.35 \times 10^{-3}$. The results are shown in Fig. 4.

C. The same voltage program was used as in case A except lowering the voltage at transition, i.e., following curve C of Fig. 2. In this case, beam loss jumps to about 15%. The increase in the beam area and the final momentum spread are slightly less than those in case A. The results are shown in Fig. 5.

D. As seen from Eq. (7), the nonlinear effect of the momentum spread can be overcome by introducing into the ring the sextupole elements which can be pulsed on during transition to make $\alpha_2 = -1.5$. Using the voltage programs described above to study such a case, we found that particle losses were reduced to 7%, 0.6% and 11% for cases A, B and C, respectively, and the beam phase-space area and the final momentum spread also decreased slightly from their corresponding cases. Hence, the effect on the phase motion due to nonlinear rf forces alone is quite significant.

E. We can take case D a step further by making α_2 to be, say, -4.5. (This can be accomplished by introducing in the ring a 2.4 m sextupole with a half aperture 5.4 cm and pole tip field of 5 kG.) Following the voltage program of case A, we found that the combined nonlinear effects could actually reduce the mismatch of the beam after transition. The results show that the beam loss is reduced to about 4%, and the beam area increase and the final momentum spread are also slightly less than those in cases A and D.

Some conclusions can be drawn from these computer experiments. The nonlinearities mainly cause the beam to be mismatched after transition, and, in turn, enhance the filamentation in the phase space. This could result in an excessive beam loss unless a bigger rf bucket is provided after transition. In order to minimize such a mismatch, a higher voltage should be used at transition, along with some kind of modification of α_2, if possible.

Acknowledgment

The author wishes to thank Dr. L.C. Teng for his help and advice during the course of this study.

Appendix

The hamiltonian for the longitudinal phase motion is

$$H(\psi,\bar{w};t) = \frac{1}{2}\frac{\Lambda}{\gamma_s}\bar{w}^2 + \frac{1}{3}\beta_s\left[\frac{3/2}{\gamma_s^4} + \frac{\alpha_2+3\Lambda/2}{\left(\gamma_s^2-1\right)\gamma_t^2}\right]\bar{w}^3$$

$$- \frac{1}{2\pi h}\frac{ev}{mc^2}\left[\psi \sin \phi_s + \cos\left(\phi_s+\psi\right)\right] \qquad \text{(A1)}$$

where H is in mc^2 units. In the adiabatic region where the hamiltonian is conservative, the four fixed points for the motion occur at $d\bar{w}/dt = 0$ and $d\psi/dt = 0$. The two unstable fixed points, in turn, give two distinct separatrices (or buckets). In regions far from transition, one of the separatrix is usually outside the vacuum chamber. Assuming there exists an instantaneous constant hamiltonian in the nonadiabatic region, Kolomenski and Sabsovich[5] have studied the evolution of these two separatrices passing through transition. We repeated their calculation here for case A, taking into account the combined nonlinear effects. The results are shown in Fig. 6, where the separatrix is represented by solid curves and the beam by shaded areas. Since the beam passes through transition rather rapidly for our case, the trajectories of the particles have no time to be altered substantially. Nevertheless, these pictures give us some idea of transition crossing.

References

1. S.C. Snowdon, "Determination of Booster Magnet Sextupole Strength," NAL report TM-156/0320 (March, 1969).
2. J.A. MacLachlan, "RF Capture in the NAL Booster," NAL report TM-303/0330 (May, 1971).
3. S.C. Snowdon, "Booster Constant Bucket Area Regime with Space Charge," NAL report TM-304/2000, 5000 (May, 1971).
4. K. Johnsen, "Effects of Nonlinearities on the phase Motion," Proceedings of CERN Symposium, pp. 106-109 (1956).
5. A.A. Kolomenski and L.L. Sabsovich, "On the Decay of the Passage through the Transition Energy in Accelerators," Proceedings of CERN Symposium, pp. 112-117 (1956).

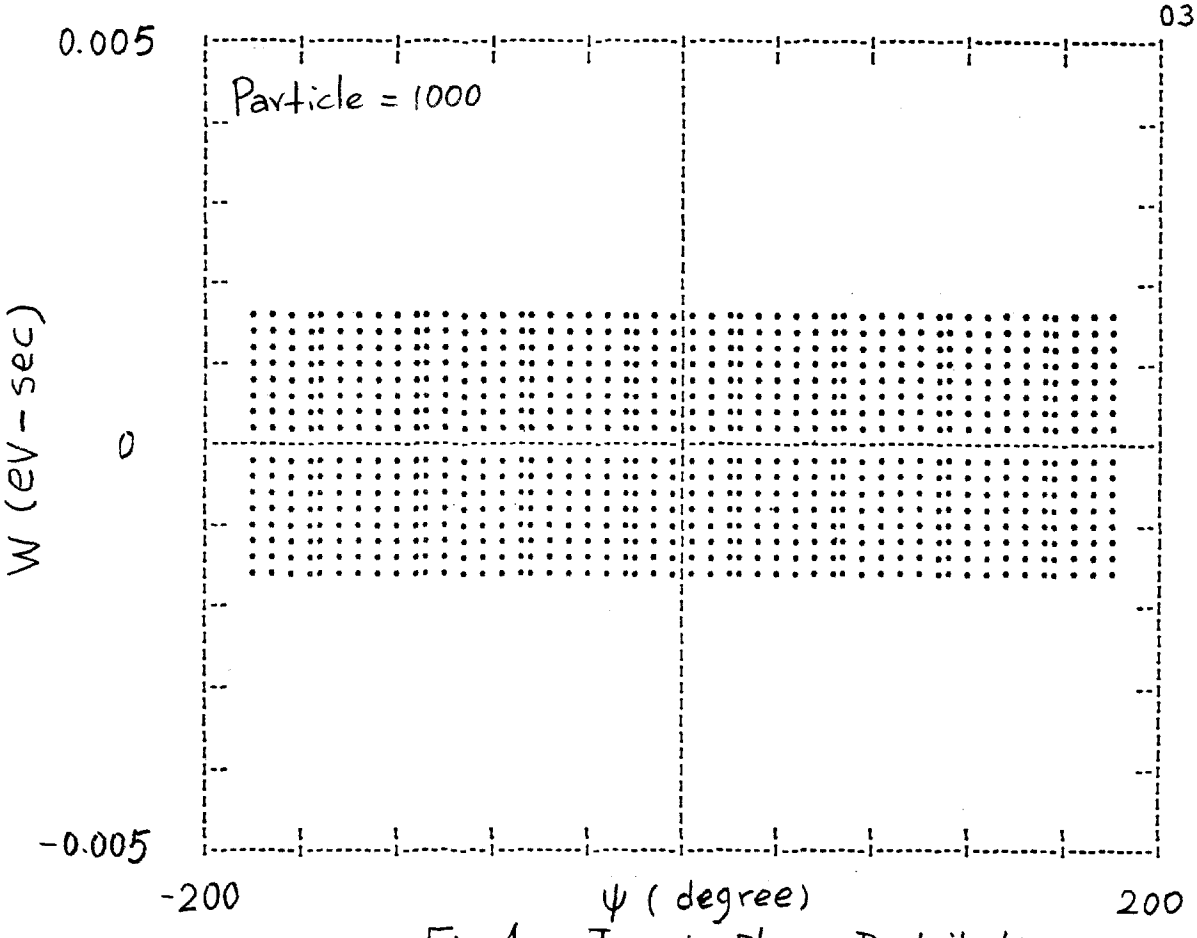

Fig. 1a Input Phase Distribution

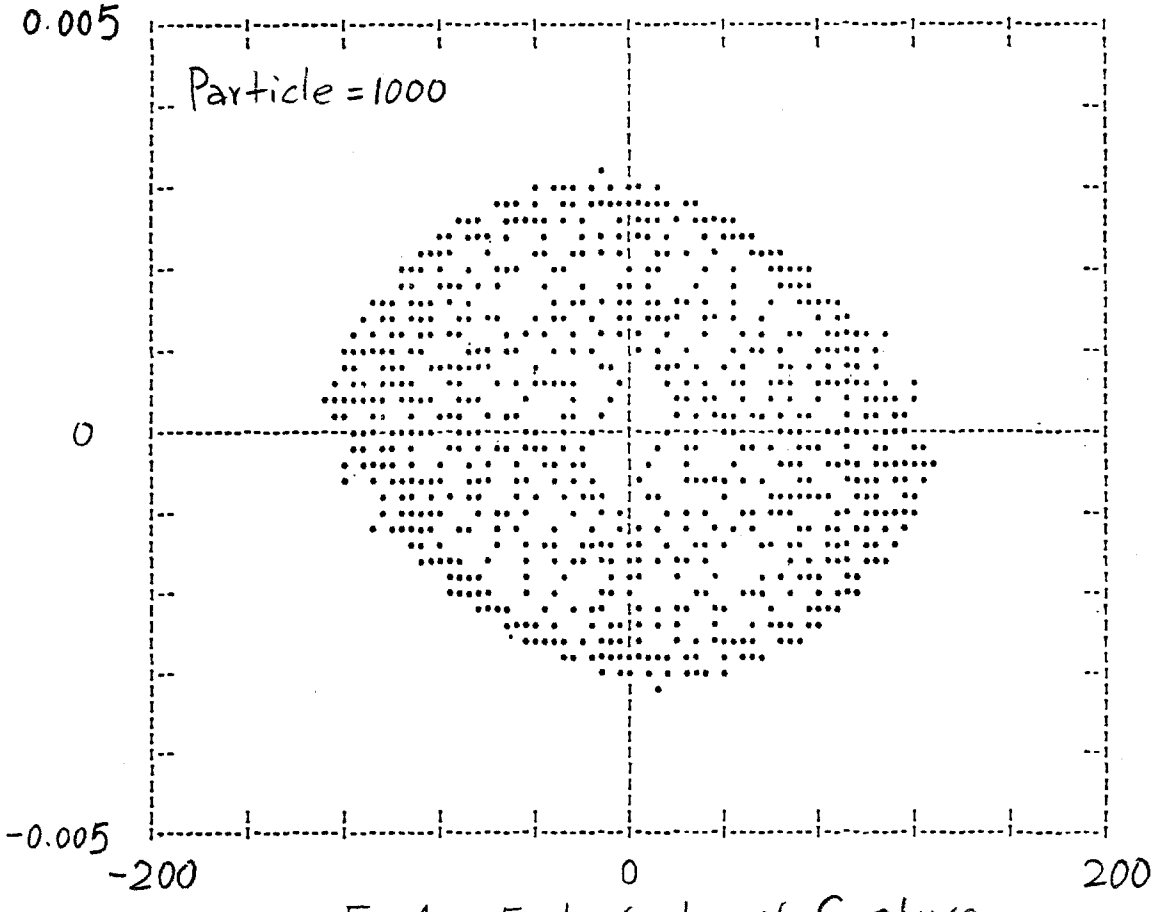

Fig. 1b End of the rf Capture

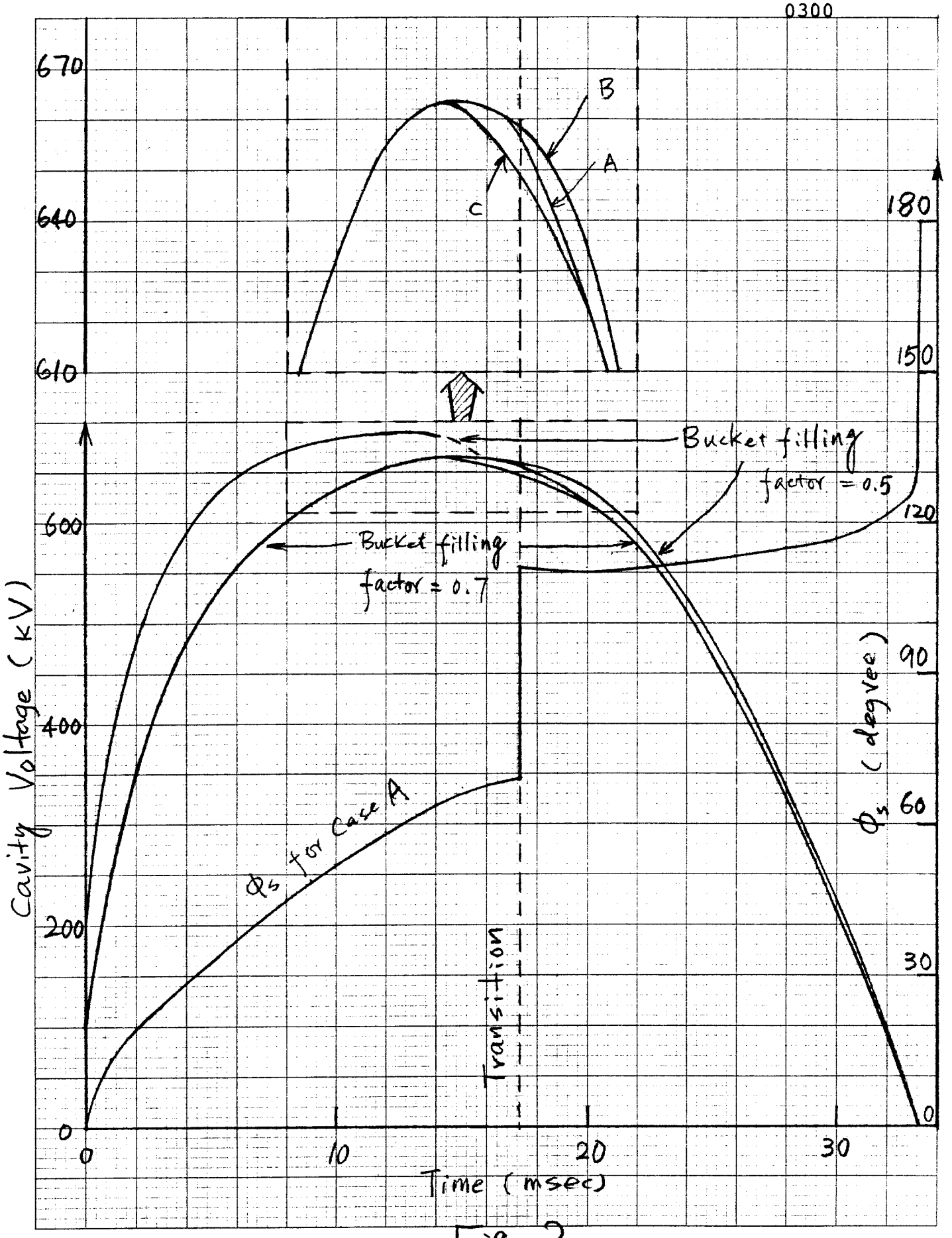
670
640
610
600
400
200
0
Cavity Voltage (kV)
180
150
120
90
60
30
0
ϕ_s (degree)
B
A
C
Bucket filling
factor = 0.5
Bucket filling
factor = 0.7
ϕ_s for case A
Transition
0
10
20
30
Time (msec)

Fig. 2

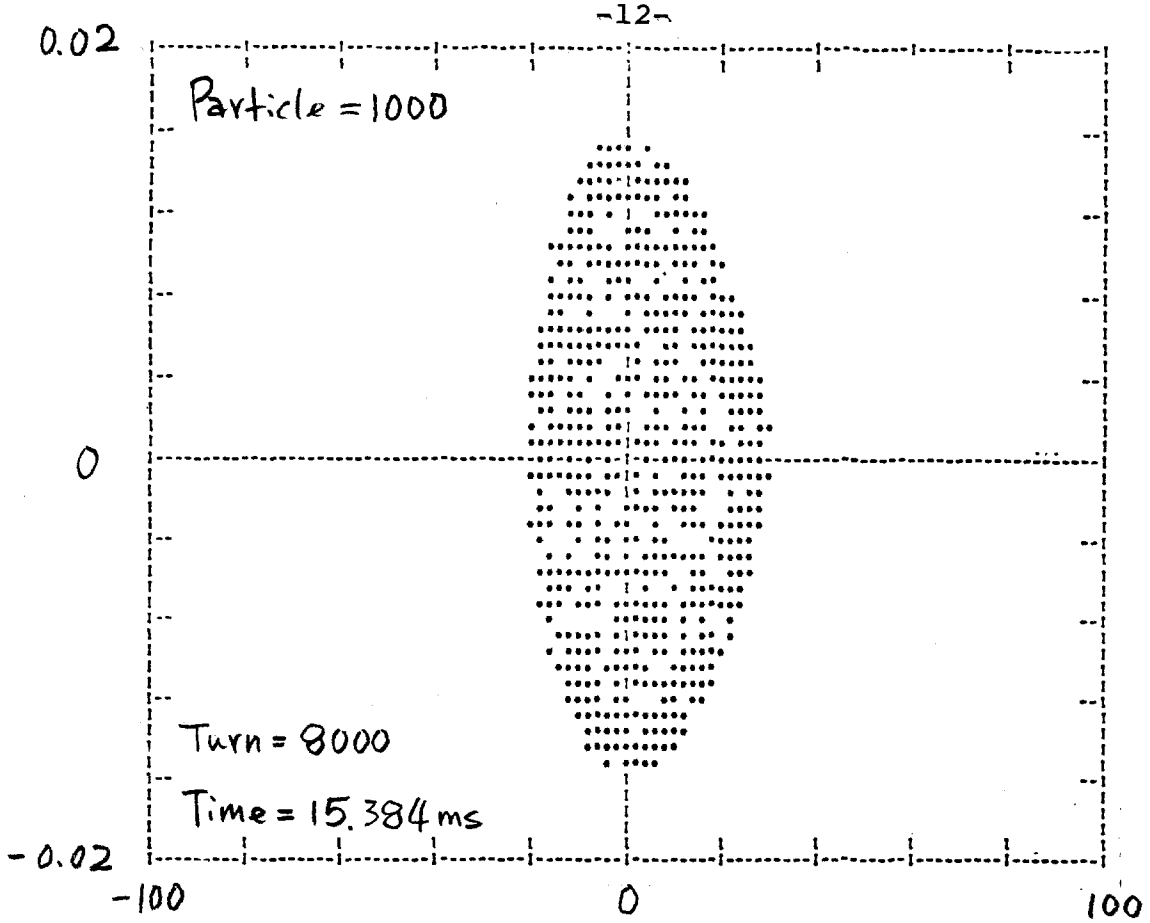

Fig. 3a

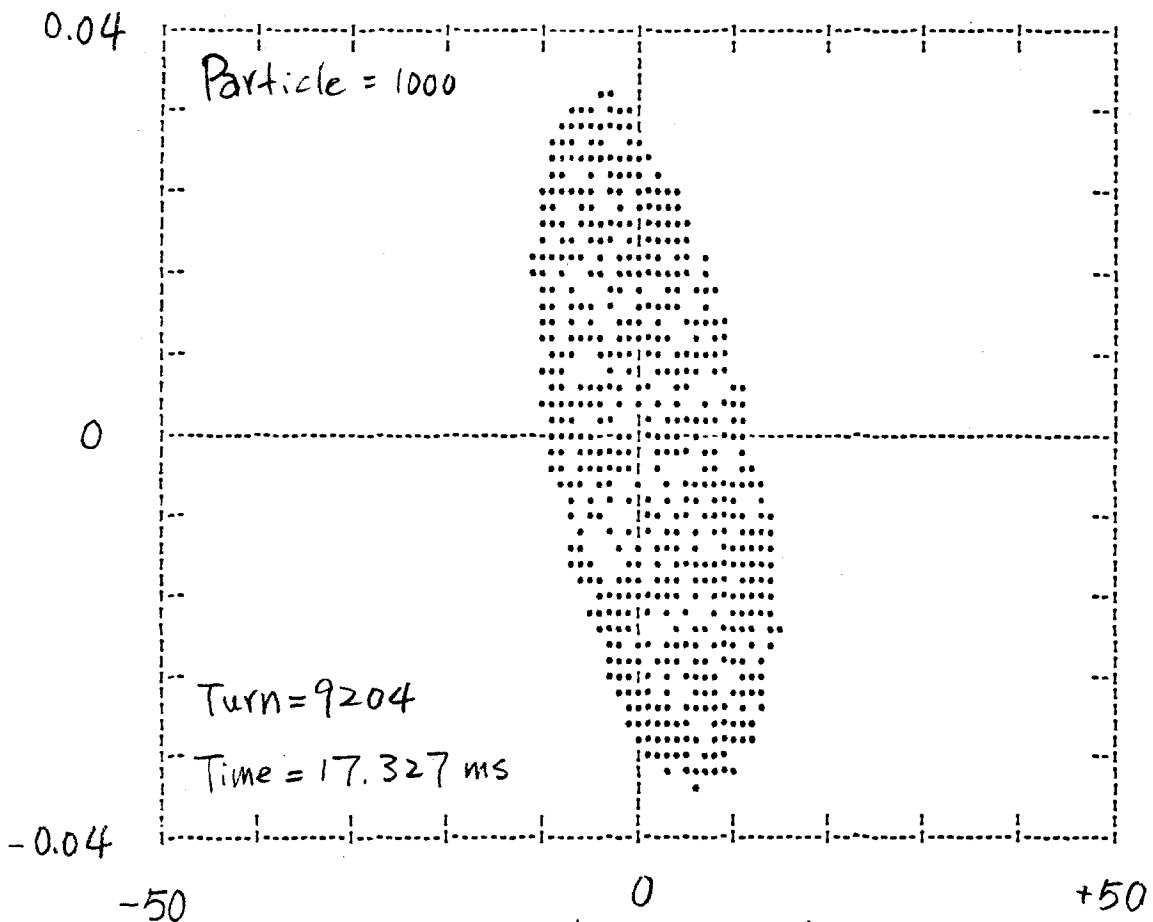

Fig. 3b Transition

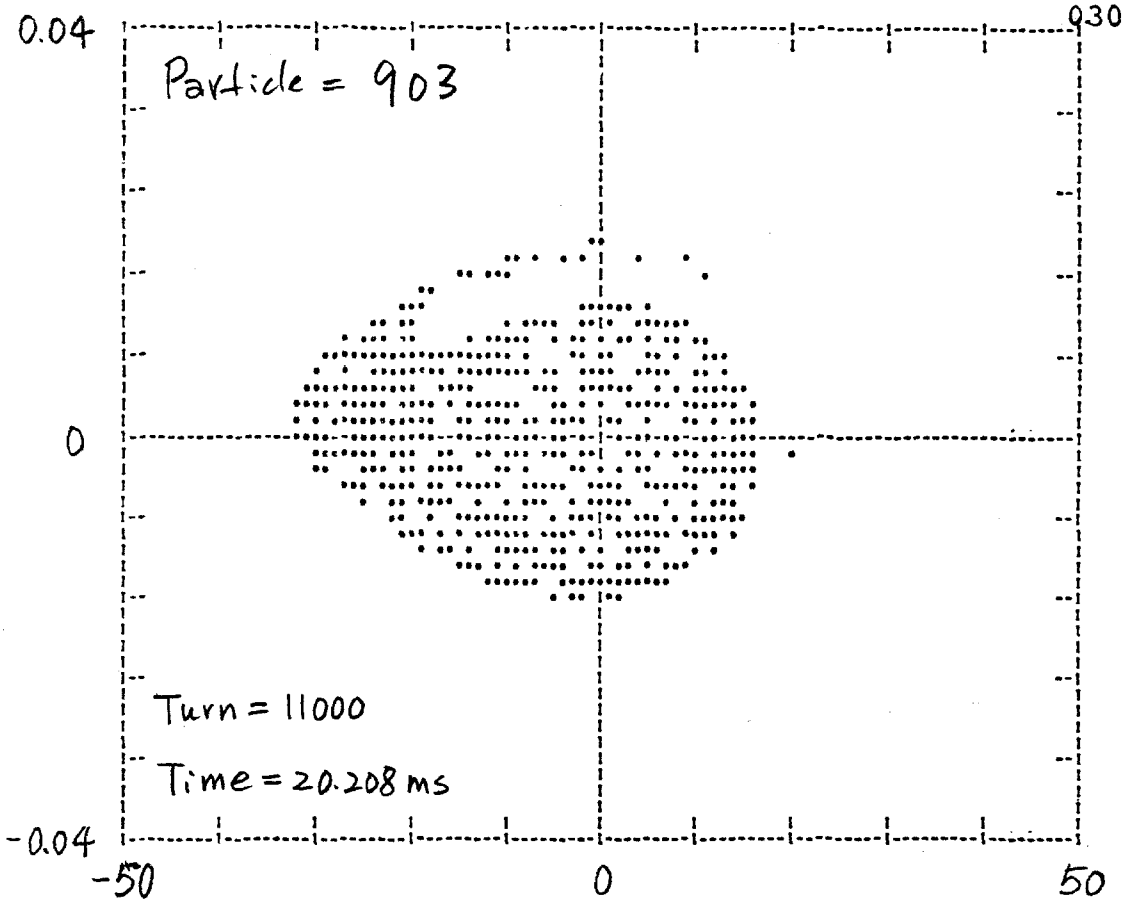

Fig. 3c

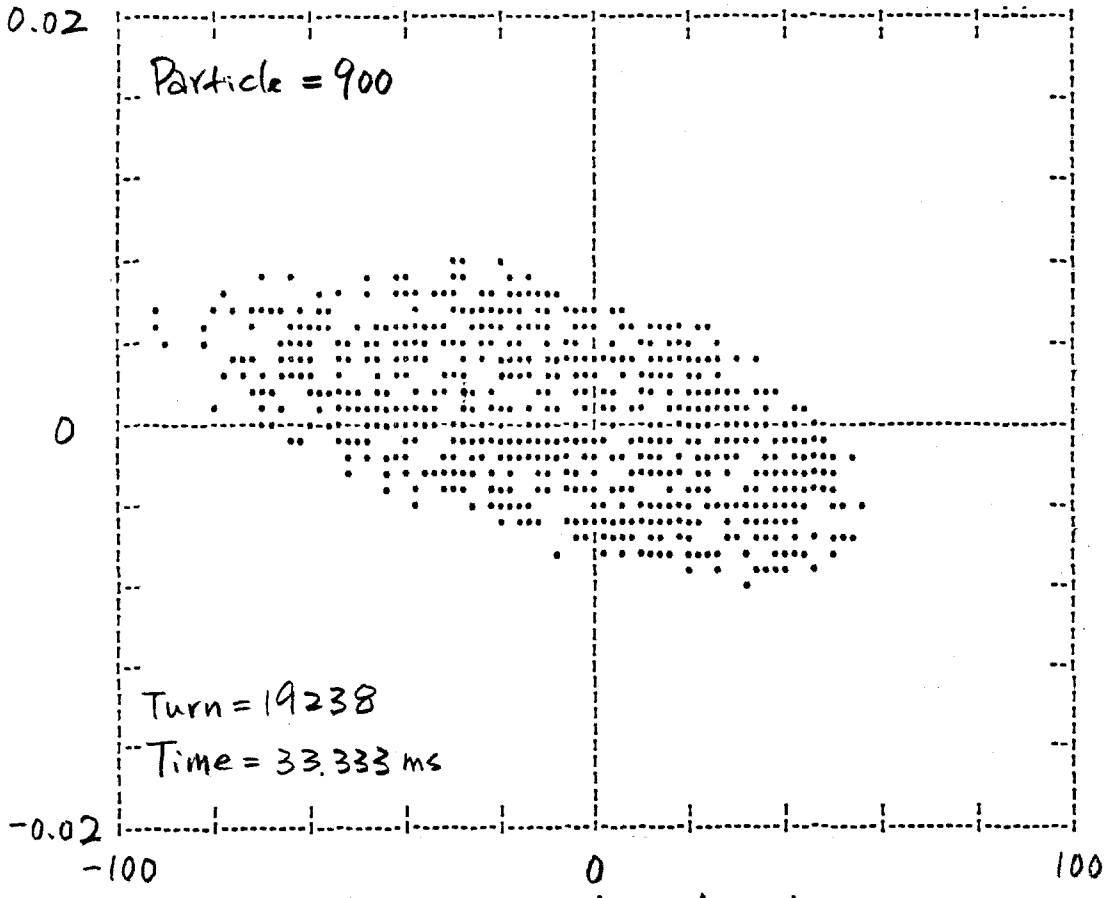

Fig. 3d End of Acceleration

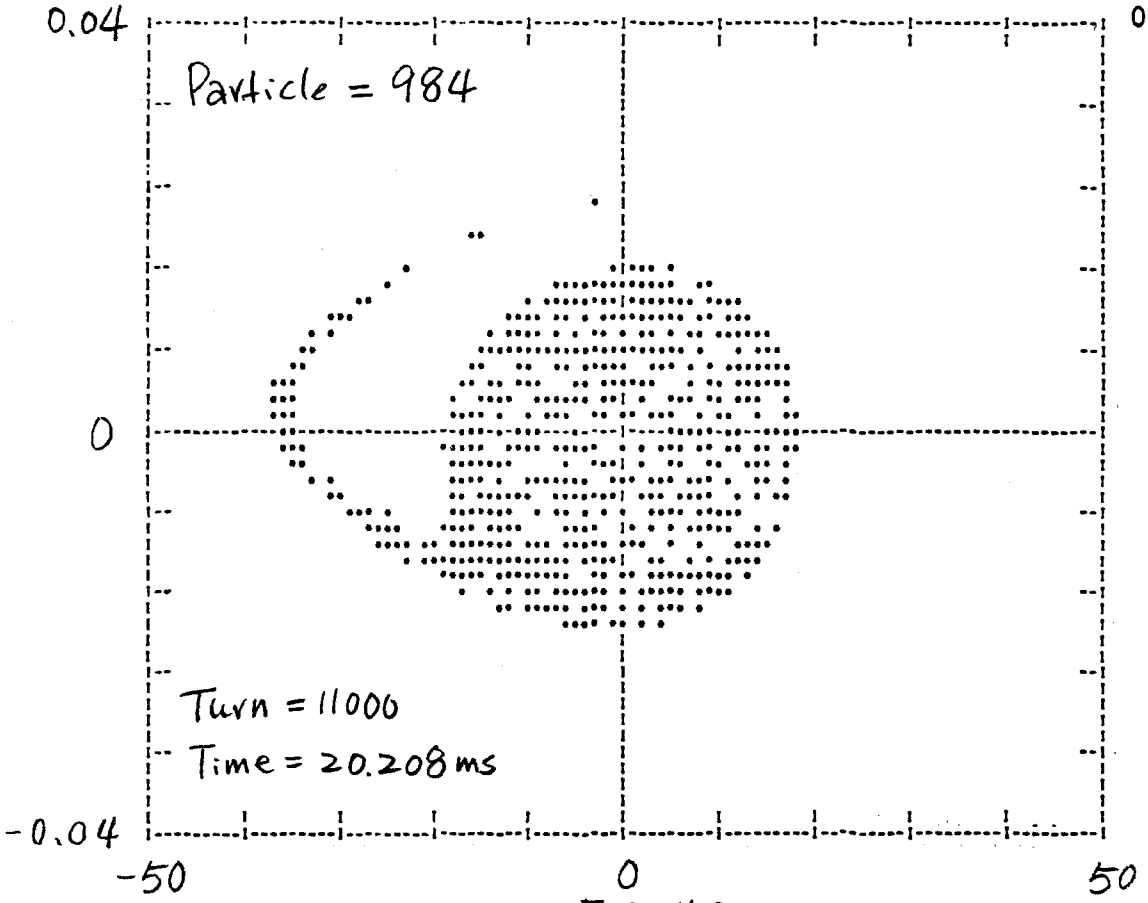

Fig. 4a

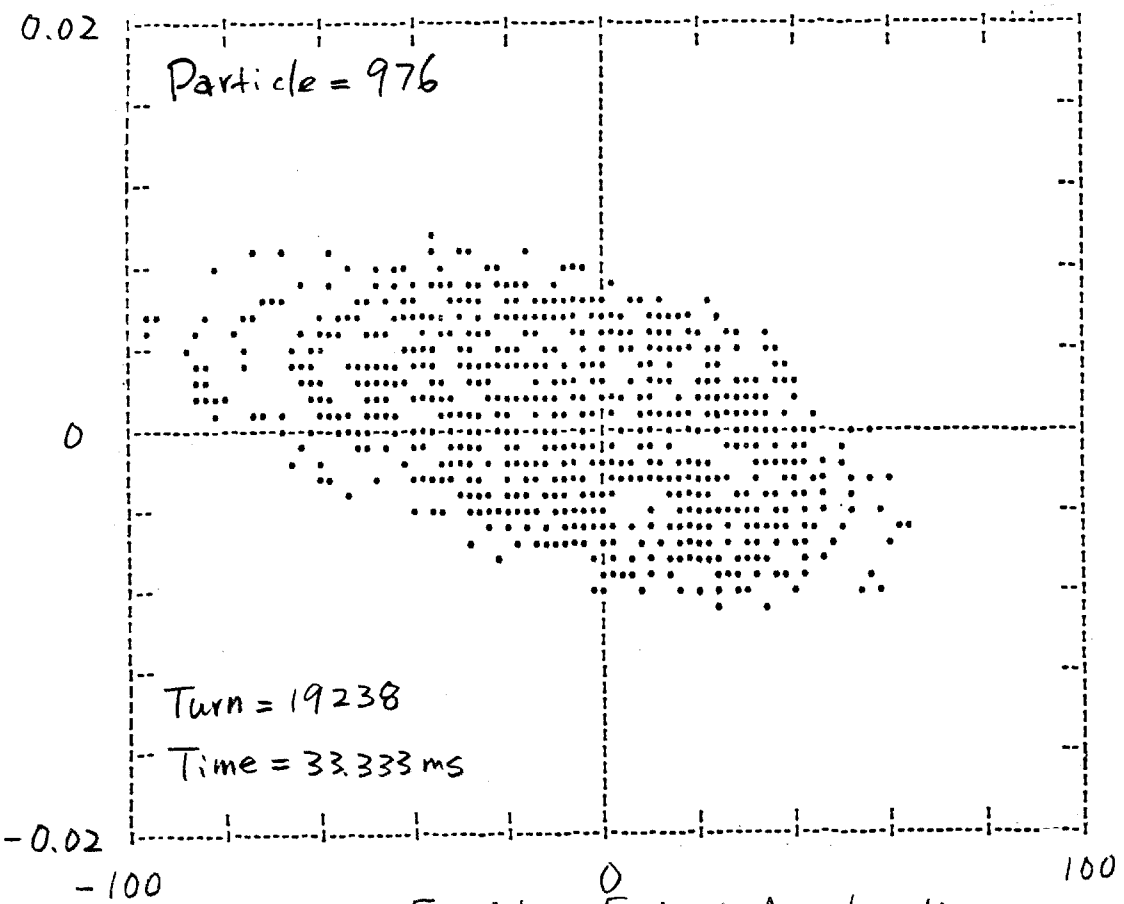

Fig. 4b End of Acceleration

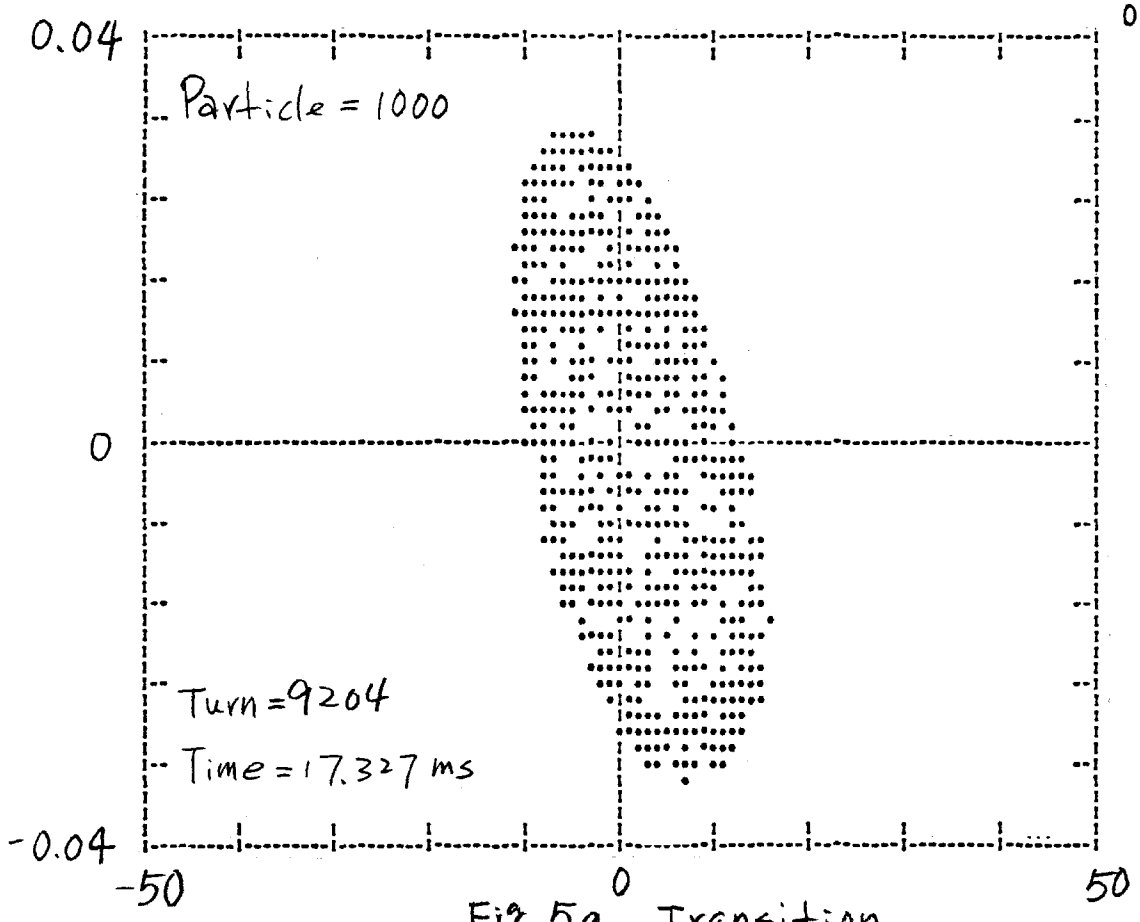

Fig. 5a Transition

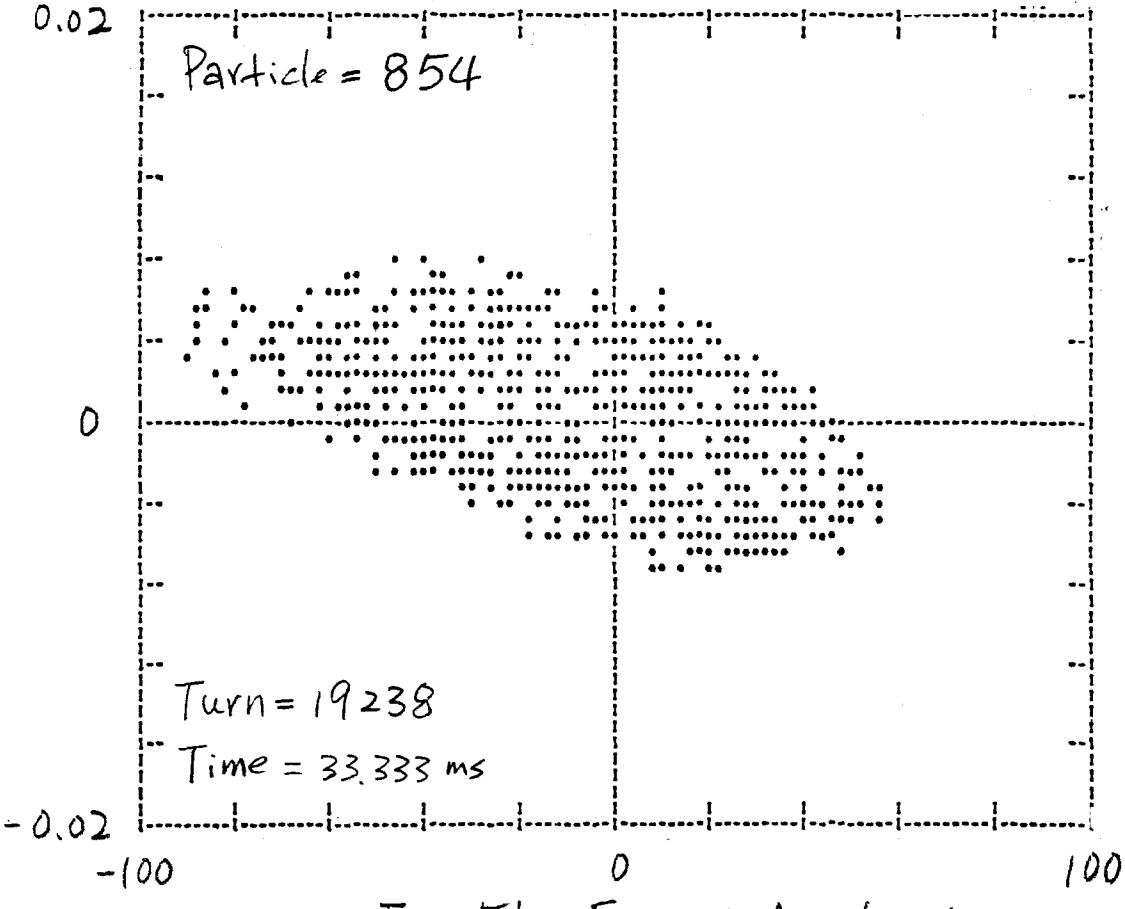

Fig. 5b End of Acceleration

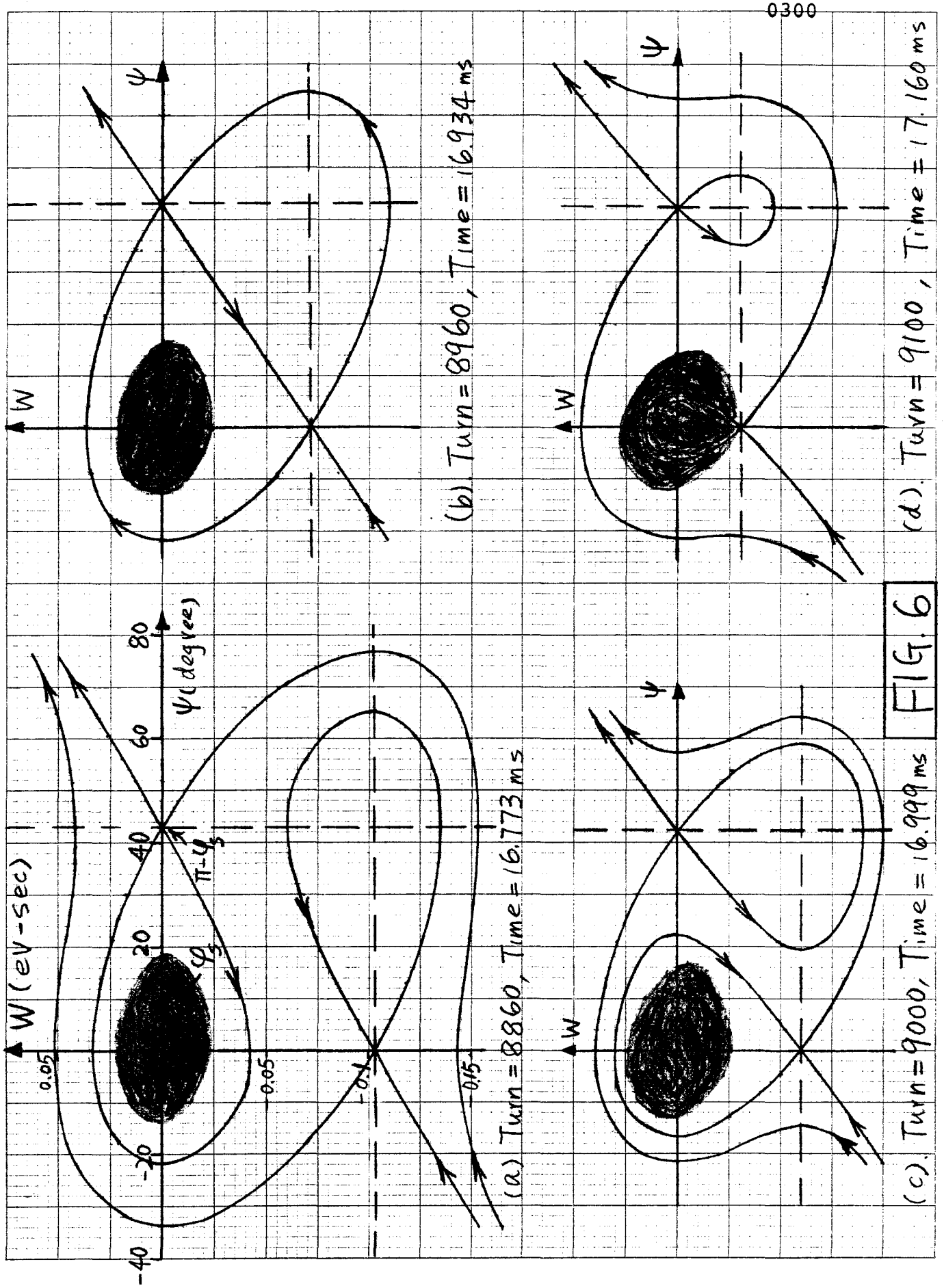
W (eV-sec)
ψ (degrees)
ψ
W
0.05
-0.05
-0.1
-0.15
-40
-20
20
40
60
80
φ_s
$\pi-\varphi_s$
(a) Turn = 8860, Time = 16.773 ms
(b) Turn = 8960, Time = 16.934 ms
(c) Turn = 9000, Time = 16.999 ms
(d) Turn = 9100, Time = 17.160 ms

FIG. 6

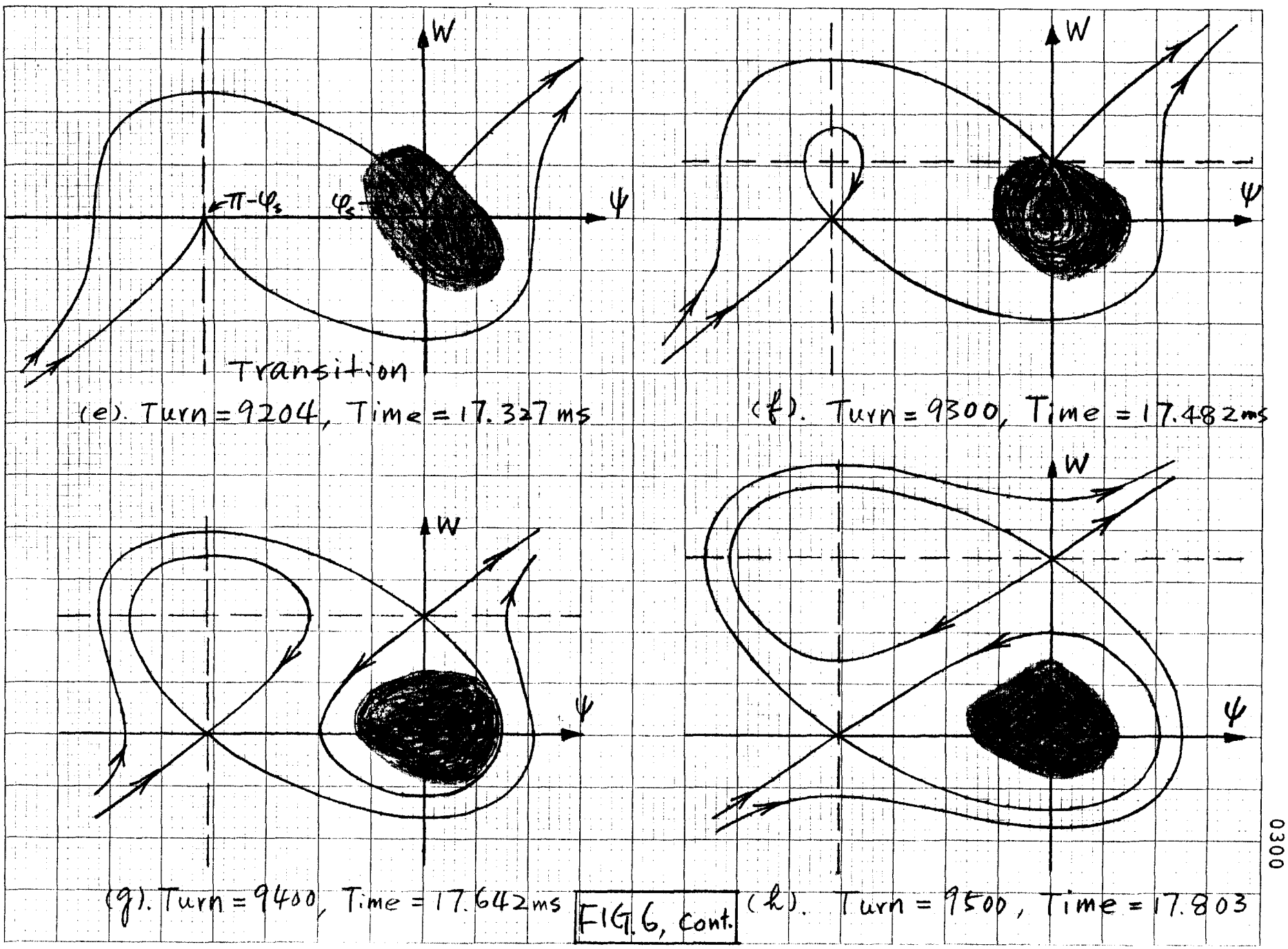
W
ψ
π-φs
φs
Transition
(e). Turn = 9204, Time = 17.327 ms
(f). Turn = 9300, Time = 17.482 ms
(g). Turn = 9400, Time = 17.642 ms
(h). Turn = 9500, Time = 17.803

FIG. 6, Cont.

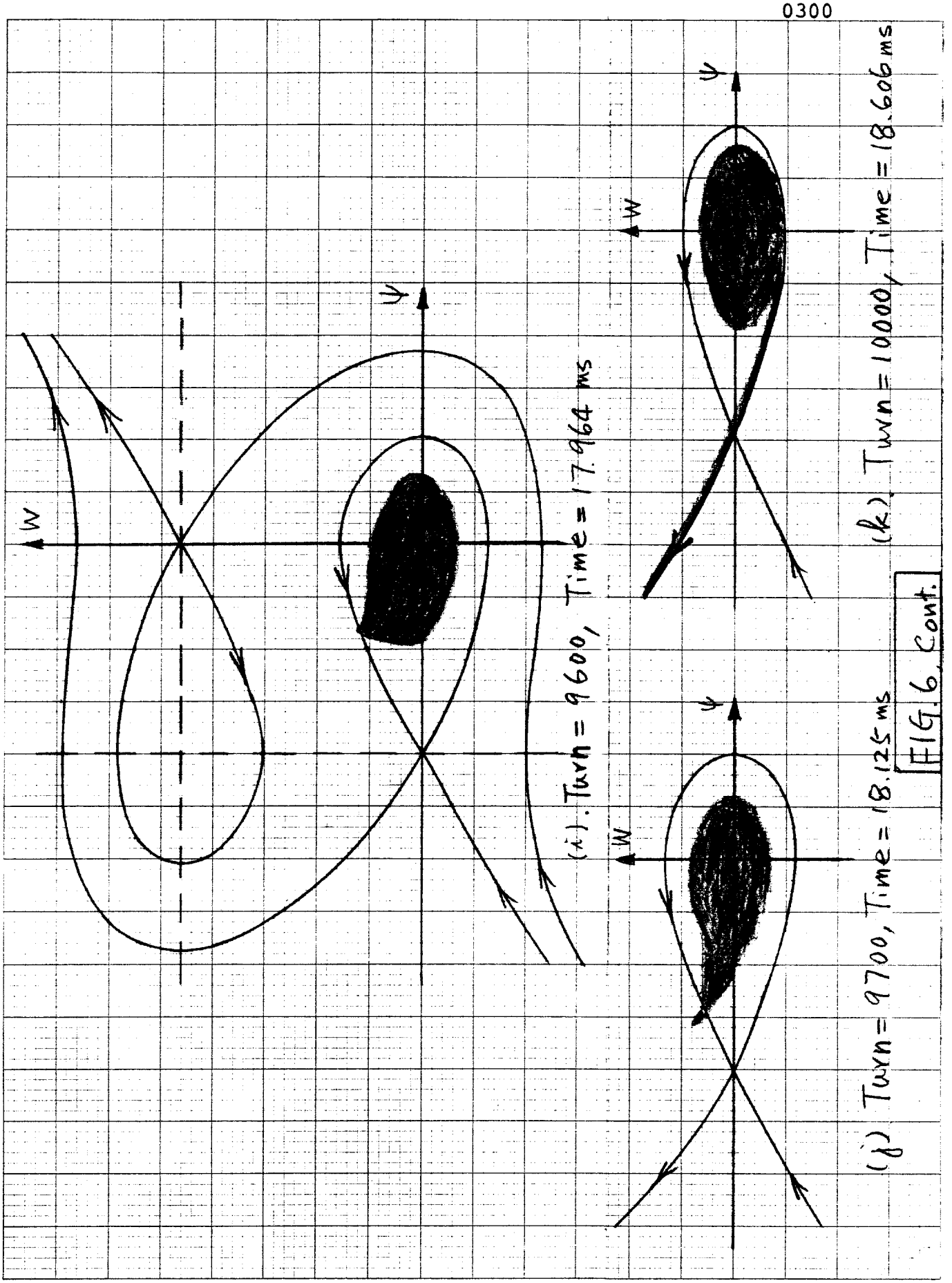
ψ
W
(i). Turn = 9600, Time = 17.964 ms
ψ
W
(j) Turn = 9700, Time = 18.125 ms
ψ
W
(k). Turn = 10000, Time = 18.606 ms

FIG. 6 Cont.